URSI GASS 2020, Rome, Italy, 29 August - 5 September 2020

Dust Charge Modeling and Ejecta Measurements for Hypervelocity Impacts on Aluminum and Powdered Regolith Simulant Targets

Gil Shohet*(1), Nicolas Lee(1), and Sigrid Close(1)
(1) Department of Aeronautics & Astronautics, Stanford University, Stanford, California, USA, 94305

Abstract

Meteoroid and space debris impacts on spacecraft pose an electrical threat due to the electromagnetic pulse (EMP) and radio frequency (RF) emissions produced by the impact-generated plasma. Charge attachment to macroscopic particles ejected from the impact crater affects plasma measurements in ground based experiments, and may lead to a dusty plasma. We find that the ejecta curtain from light gas gun impacts aligns with plasma measurements indicative of charged dust. Combining experimental measurements of the ejecta particle size distribution with a dust model based on an extended orbital motion limited (OML) theory, we estimate the extent of charge attachment in the ejecta curtain passing through the post-impact plasma plume. Given the measured particle size distribution, we show that significant charge attachment and localized electron depletion may occur at early time, and that, depending on material properties, thermionic emission may result in a dust population whose electrical charge changes sign over time. These results suggest that ejecta charging can play a significant role in the evolution of impact plasmas.

1 Introduction

Spacecraft are routinely bombarded by particles, such as meteoroids and space debris, traveling between a few and tens of km/s. These impacts are termed hypervelocity because they occur at speeds faster than the material speed of sound, resulting in hydrodynamic behavior. On impact, the projectile and part of the target are vaporized and partially ionized, forming a dense plume of neutral gas, plasma, and macroscopic condensed phase material that expands into the vacuum. Instabilities and oscillations in the expanding plasma result in radio frequency emissions and a broadband EMP that have the potential to cause electrical damage [1].

Due to interactions with the plasma, macroscopic ejecta particles, referred to as "dust," acquire a surface charge. Charged dust has been measured in ground-based hypervelocity impact experiments, and may be a source of macroscopic charge separation and long-range elecromagnetic fields [2]. References to the impact plasma as "dusty" date back over thirty years, but the effects of dust remain elusive due to insufficient experimental data and the lack of a rigorous theoretical framework to model dust charging in the impact environment. A key question is whether there is a true dusty plasma versus dust in plasma; that is, whether there is sufficient charge attachment for collective behavior, or whether the ejecta can be treated as isolated particles immersed in the plasma.

First, we present a theoretical framework for modeling charge attachment across the length and time scales spanned by the expanding plasma. Second, we present results from a recent light gas gun impact campaign at the NASA Ames Vertical Gun Range (AVGR), including thin-film witness plate measurements of microscopic ejecta. We make the first measurements of microscopic debris from an aluminum-on-aluminum impact. Finally, we combine the dust model with a simplified model of the post-impact environment to make preliminary estimates of charge attachment, and consider the ramifications for experimental observations. We particularly focus on impacts on aluminum and regolith targets as analogues for impacts on spacecraft and small solar system bodies bodies, respectively.

2 Dust Charging Theory

We model the charging and dynamics of dust grains with an extended orbital motion limited (OML) framework based on dust charging and transport models developed for Tokamak plasmas (see Ch. 1 of [3] for a thorough summary). The OML fluxes are given by the functional

$$\mathscr{I}_\alpha[\mathfrak{v}] = \int_{v_{\min}}^{\infty} \mathfrak{v}\sigma_\alpha^{\mathrm{d}} f_\alpha(v_\alpha)\,\mathrm{d}v_\alpha, \tag{1}$$

where for particle of species α and charge q_α, and dust with radius r_{d} and surface potential ϕ_{d}, we have the OML collisional cross-section $\sigma_\alpha^{\mathrm{d}} = \pi r_{\mathrm{d}}^2\left(1 - 2q_\alpha\phi_{\mathrm{d}}/m_\alpha v_\alpha^2\right)$ and lower integration bound $v_{\min}^2 = \max\left(0,\, 2q_\alpha\phi_{\mathrm{d}}/m_\alpha\right)$.

The dust charge Q_{d}, velocity $\boldsymbol{v}_{\mathrm{d}}$, temperature T_{d}, and mass M_{d} evolve according to the system of ODEs

$$\dot{Q}_{\mathrm{d}} = \sum_\alpha \mathscr{I}_\alpha[q_\alpha v_\alpha] + I_{\mathrm{th}} + I_{\mathrm{see}} \tag{2}$$

$$M_{\mathrm{d}}\dot{\boldsymbol{v}}_{\mathrm{d}} = \sum_\alpha \mathscr{I}_\alpha[m_\alpha \boldsymbol{v}_\alpha v_\alpha] + F_{\mathrm{coulomb}} \tag{3}$$

$$M_{\mathrm{d}}\dot{H}_{\mathrm{d}} = \sum_\alpha \mathscr{I}_\alpha\left[m_\alpha v_\alpha^2/2 - q_\alpha\phi_{\mathrm{d}}\right] + P_{\mathrm{surf}} + P_{\mathrm{loss}} \tag{4}$$

$$\dot{M}_{\mathrm{d}} = \Gamma_{\mathrm{abl}} + \Gamma_{\mathrm{acc}}, \tag{5}$$

where the OML terms can be integrated analytically assuming a drifting Maxwellian plasma. Dust charging occurs due to the OML fluxes and thermionic and secondary emissions. Drag is caused by OML momentum fluxes and coulomb drag from ions. The energy balance consists of the OML kinetic energy flux and additional terms $P_{\rm surf}$, which includes thermalization and neutralization at the surface, and $P_{\rm loss}$, which includes energy loss to blackbody radiation, thermionic and secondary emissions, and ablation. We relate the specific enthalpy $H_{\rm d}(T_{\rm d})$ to the temperature by a material model. Finally, the mass evolves due to loss from ablation ($\Gamma_{\rm abl}$) and growth from like particle fluxes to the surface ($\Gamma_{\rm acc}$). These processes are illustrated in Figure 1.

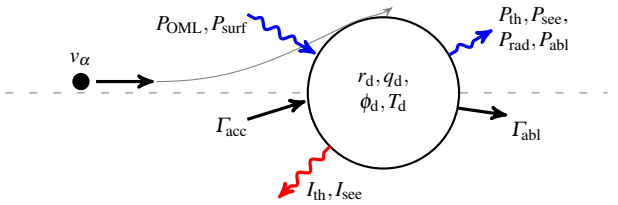

Figure 1. Schematic of the extended OML model showing a grazing collision, annotated with additional terms.

Although OML theory has the advantage of providing closed-form analytic expressions for the fluxes, the inherent assumption of $r_{\rm d} \ll \lambda_{\rm De} = \sqrt{\varepsilon_0 k_{\rm B} T_{\rm e}/n_{\rm e} e^2}$ is flagrantly violated in the first few microseconds after impact due to the initial plasma density of $n_e \sim 10^{23}$ m^{-3} [4]. OML neglects screening effects and thus significantly underestimates the surface charge. OML can be extended to $r_{\rm d} \sim \lambda_{\rm D}$ by accounting for the plasma response with a modified Whipple approximation relating the surface potential and charge [5],

$$Q_{\rm d} = 4\pi\varepsilon_0 r_{\rm d}\,(1 + r_{\rm d}/\lambda_{\rm s})\,\phi_{\rm d}, \tag{6}$$

where $\lambda_{\rm s}^{-2} = \lambda_{\rm De}^{-2} + \lambda_{\rm Di}^{-2}$. Neglecting additional terms, and assuming $r_{\rm d} \ll \lambda_{\rm D}$ and $m_{\rm i} = m_{\rm p}$, the OML equilibrium solution is $e\phi_{\rm d} = -2.5 k_{\rm B} T_{\rm e}$, so to first order the dust charge depends *linearly* on the dust radius and plasma temperature.

3 Experimental Observations

A number of previous hypervelocity impact studies have aimed to characterize macroscopic and microscopic debris from impacts on targets made from geologic materials (see, for example [6, 7]), and more recently macroscopic fragments ($d \gtrsim 0.3$ mm) from aluminum targets [8]. The cumulative distribution of ejected particles with diameter $d_{\rm p}$ greater than d is typically modeled as a power law with coefficient C and exponent D,

$$N(d_{\rm p} > d) = C d^{-D}, \tag{7}$$

where typically $1.5 \lesssim D \lesssim 3.0$, depending on impact conditions and material choice. Given that the marginal abundance of particles follows a $-(D+1)$ power law, and attached charge scales linearly with radius, we expect small ejecta particles to carry the bulk of attached charge.

To characterize the microscopic ejecta, we use a witness plate design similar to [6]. We placed 1 μm thick Mylar films concurrently with Faraday cup plasma sensors [9] at various locations approximately 1 m from the impact site. We process the witness plates by taking photographs through a polarizing microscope with a 20x objective, identifying holes manually, and measuring the cross-sectional area using image processing methods. We are able to identify holes slightly smaller than 1 μm in diameter.

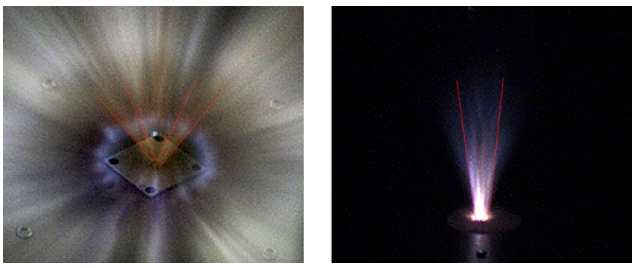

Figure 2. High speed camera images from an aluminum impact (left) and the regolith simulant impact (right). The approximate ejection angles are marked in red.

Based on high speed imagery (Figure 2), which show that the macroscopic ejecta curtain for impacts on aluminum and regolith simulant targets, respectively, is concentrated at a 60° and 90° elevation angle, we focus our hole counting efforts at these respective locations. We also see evidence of charged dust impacts in the form of impulsive current measurements in the colocated plasma sensors. Interestingly, both our work and experiments by Crawford and Schultz [2] show evidence of positively charged ejecta in plasma data from regolith impacts, but we predominantly see evidence of negatively charged ejecta for the aluminum impacts. In the following section we describe the effect of thermionic emission, which may be responsible for this result.

Due to low debris production from the aluminum targets, we average the integrated ejecta counts from three impacts from 4.97 to 5.41 km/s. The impact velocity into the regolith simulant was 5.56 km/s. All shots used 1.6 mm aluminum projectiles. We present measurements of the cumulative particle size distribution for these two cases in Figure 3. Data from the regolith impact show reasonable agreement with previous experiments on powdery targets [6].

We find that the cumulative particle size distribution for the regolith impact follows a power law with exponent $D = 2.07$, and for the aluminum impacts exponent $D = 1.48$. Because larger holes are easier to identify than smaller holes, we suspect there is a minor systematic undercount of the small ejecta. The small absolute count of large holes may also bias the results. A thorough uncertainty and error analysis is ongoing.

4 Modeling Results

To model dust charging, we require a model for the post-impact environment. The impact and subsequent expan-

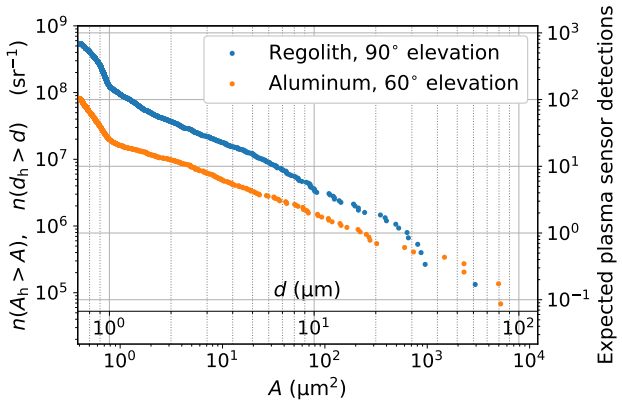

Figure 3. Measured hole size distribution for impacts on regolith and aluminum targets, normalized by solid angle and by the expected number of plasma sensor detections.

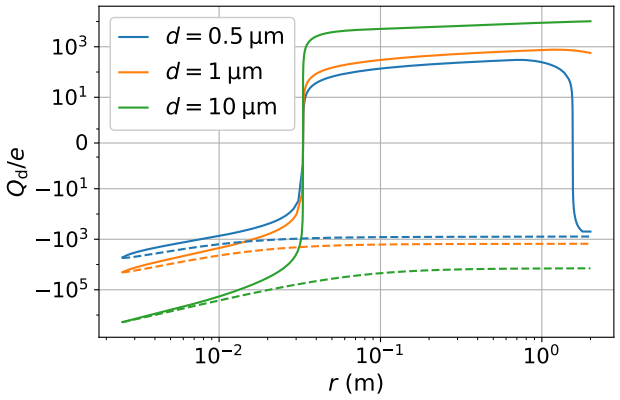

Figure 4. Charge as a function of distance from impact site for particles from 0.5 to 10 μm in diameter. Solid lines use equation 4, while the dashed lines show the effect of reducing the OML heating term by a factor of 100.

sion are complex, anisotropic processes spanning many orders of magnitude in space and time, and multiple physical regimes. For tractability, we use a simplified one-dimensional model for cratering and plasma evolution based on [1] and [10]. In particular, we estimate the charge production using $Q = 0.1\,m\left(m/10^{-11}\right)^{0.02}(v/5)^{3.48}$, and the crater size using $r_c = k\,m^{0.352}\,\delta^{0.167}\,v^{0.667}$. Here, Q is the charge produced in C, m is the projectile mass in g, v is the projectile velocity in km/s, r_c is the crater depth in cm, δ is the projectile density in g/cm^3, and k is a material constant (0.42 for aluminum). We assume that the plasma formation time is less than the dust ejection time, and that the dust travels through a fully-formed plasma with profile

$$n_e(r) = \left(\frac{r_c}{r}\right)^3 \frac{Q}{eV_c}\left(1+\frac{v_{exp}D_p}{v_p r_c}\right)^{-3}, \qquad (8)$$

where r is the distance from the impact site, V_c is the crater volume, v_{exp} is the expansion velocity, v_p is the projectile velocity, and D_p is the projectile diameter.

We consider an aluminum target impacted by a 1.6 mm diameter (5.8 mg) aluminum projectile traveling at 5.25 km/s. To identify general trends, we assume singly charged aluminum ions with $n_i = n_e$ and $T_i = T_e = 1$ eV, that throughout the expansion $n_{n,Al} = 100\,n_e$, and an expansion velocity of 10 km/s. This results in a plasma density of $O\left(10^{22}\right)$ m^{-3} initially that drops to $O\left(10^{14}\right)$ m^{-3} in the neighborhood of the sensors. The assumptions smooth over hydrodynamic and plasma effects, but are a reasonable first-order approximation of the densities and temperatures observed in light gas gun impacts [4, 9, 10]. Finally, because the AVGR environment is at a low vacuum, we include a stationary neutral background at the background pressure of 0.5 Torr. We use an implicit Adams-BDF method to integrate the dust charging and dynamics model in equations (2)-(5).

We find the evolution of dust particles displays a complex dependence on the initial conditions, plasma parameters, prescribed neutral background, and material properties. However, for reasonable inputs, we obtain dust transit times of 300-2000 μs, in agreement with plasma measurements. We show representative charging trends for an aluminum impact in Figure 4. Due to drag from the neutral background stopping very small particles, the model suggests a minimum diameter of approximately 0.1-0.5 μm for dust particles to reach the plasma sensors. The charging time scales are sufficiently fast that the dust charge can be estimated by setting the left-hand-side of equation (2) to zero; however, the dust grain is not necessarily in thermal equilibrium once it has traveled a few crater radii.

A major source of ambiguity is the role of heating due to the OML component of equation (4). Studies of dust in Tokamaks have shown that OML theory greatly overestimates heating under certain conditions because it neglects shielding from particles ablating off the dust grain [3]. The level of heating not only affects the magnitude of charging and degree of ablation, but also whether we predict positively charged dust due to thermionic emission. Moreover, Figure 4 indicates that the charge may switch signs multiple times, and sensor location may play a role in the sign of charge detected. The presence of a neutral background also affects the degree of ablation and whether positive charging occurs, adding an additional layer of complexity.

Combining the dust charging model with the measured ejecta distribution, we can make predictions on the total attached charge $Q_{d,tot}$. We solve Q_{eq} by setting the left hand side of equation (2) to zero, and integrate against the marginal ejecta size distribution obtained from the derivative of equation (7),

$$Q_{d,tot} = \Theta \int_{d_{min}}^{d_{max}} CD\delta^{-(D+1)} Q_{eq}(\delta)\,d\delta, \qquad (9)$$

where Θ is the solid angle of the ejecta cloud. We model the ejecta as uniformly distributed and constrained to a hollow cone of 5° arc angle centered at a 60° elevation angle. We set d_{min} by noting that our model predicts rapid ablation of particles much smaller than 0.1 μm, and d_{max} such that the

total mass of particles under consideration approximately matches the mass ejected from the crater.

Depending on the exact bounds chosen, we predict that overall 0.1-0.3% of electrons attach to ejecta at early time for the aluminum-on-aluminum impact. For the regolith simulant target, which produces significantly more dust, the level of attachment may be even greater. The results suggest a relatively small fraction of the overall electron population is depleted due to charge attachment; however, the plasma and ejecta plumes have a strong elevation-angle dependence, and there may be localized regions with much greater charge attachment and electron depletion. Given that only a few percent charge attachment is sufficient to significantly alter the plasma dynamics, true dusty plasma effects appear likely.

5 Conclusions

Hypervelocity impacts produce a combination of plasma, gas phase, and macroscopic condensed phase ejecta. Electron attachment to the surface of these ejecta, or "dust" particles, has been noted for decades, and understanding the effects on plasma evolution is crucial for interpreting experimental results and characterizing the electrical risks posed to spacecraft by meteoroid and space debris impacts. To address this outstanding issue, we extend the OML dust charging and dynamics framework used for modeling dust in Tokamaks to the impact environment. In combination with experimental measurements, we apply the model to predict dust trajectories, charging, and ablation under light gas gun impact conditions.

Our witness plate measurements of the particle size distribution are the first measurements of the microsopic particle size distribution from a hypervelocity impact on a metal target. We find that although the aluminum target produced fewer debris compared with regolith simulant, our first order estimates suggest there is a potential for $> 0.1\%$ overall electron attachment near the crater, with potentially greater depletion in localized regions. We also note thermionic emissions may play an important, albeit perplexing role in determining the experimentally measured sign of charged dust. This work suggests that dusty plasma effects may fundamentally affect plasma evolution in the context of macroscopic impacts, such as ground-based gas gun experiments and space debris impacts. Implications for micro-meteoroid impacts, which are more prevalent, occur at higher velocities, and produce relatively more charge and fewer macroscopic debris, warrant further study. Refinements in the dust model coupled with kinetic simulations of the plasma evolution are needed to model the effects of dusty plasma phenomena on RF production.

6 Acknowledgements

This work is supported by the DOE NNSA Stewardship Science Graduate Fellowship grant DE-NA0003864 and AFOSR grant FA9550-14-1-0290. We would also like to thank the AVGR staff, Charles Cornelison, Alfredo Perez, Jon-Pierre Wiens, and Donald Bowling, for their invaluable support of the experimental work.

References

[1] S. Close, P. Colestock, L. Cox, M. Kelley, and N. Lee, "Electromagnetic pulses generated by meteoroid impacts on spacecraft," *Journal of Geophysical Research: Space Physics*, **115**, A12, December 2010, doi: 10.1029/2010JA015921.

[2] D. A. Crawford and P. H. Schultz, "Electromagnetic properties of impact-generated plasma, vapor and debris," *International Journal of Impact Engineering*, **23**, 1, pp. 169–180, 1999, doi: 10.1016/S0734-743X(99)00070-6.

[3] L. Vignitchouk, "Modelling the multifaceted physics of metallic dust and droplets in fusion plasmas," PhD Thesis, KTH, Space and Plasma Physics, 2016.

[4] Y. M. Hew, A. Goel, S. Close, and N. Lee, "Hypervelocity impact flash and plasma on electrically biased spacecraft surfaces," *International Journal of Impact Engineering*, **121**, pp. 1–11, 2018, doi: 10.1016/j.ijimpeng.2018.05.008.

[5] X. Z. Tang and G. L. Delzanno, "Orbital-motion-limited theory of dust charging and plasma response," *Physics of Plasmas*, **21**, 12, 2014, doi: 10.1063/1.4904404.

[6] A. M. Nakamura, A. Fujiwara, and T. Kadono, "Velocity of finer fragments from impact," *Planetary and Space Science*, **42**, 12, pp. 1043–1052, 1994, doi: 10.1016/0032-0633(94)90005-1.

[7] E. Buhl, F. Sommer, M. H. Poelchau, G. Dresen, and T. Kenkmann, "Ejecta from experimental impact craters: Particle size distribution and fragmentation energy," *Icarus*, **237**, pp. 131–142, 2014, doi: 10.1016/j.icarus.2014.04.039.

[8] M. Nishida, Y. Hiraiwa, K. Hayashi, and S. Hasegawa, "Scaling laws for size distribution of fragments resulting from hypervelocity impacts of aluminum alloy spherical projectiles on thick aluminum alloy targets: Effects of impact velocity and projectile diameter," *International Journal of Impact Engineering*, **109**, pp. 400–407, 2017, doi: 10.1016/j.ijimpeng.2017.08.005.

[9] B. Estacio and S. Close, "Dust and atmospheric effects on light gas gun hypervelocity impact experiments," submitted to *XXXIII URSI General Assembly and Scientific Symposium*, 2020.

[10] Y. Ju, Q. Zhang, D. Zhang, R. Long, L. Chen, F. Huang, and Z. Gong, "Theoretical model for plasma expansion generated by hypervelocity impact," *Physics of Plasmas*, **21**, 9, 2014, doi: 10.1063/1.4895592.